View metadata, citation and similar papers at core.ac.uk

brought to you by CORE

provided by Catalogo dei prodotti della ricerca

NeuroImage 222 (2020) 117244

Contents lists available at ScienceDirect

NeuroImage

journal homepage: www.elsevier.com/locate/neuroimage

Spatiotemporal dynamics of attentional orienting and reorienting revealed by fast optical imaging in occipital and parietal cortices

Giorgia Parisi[a,b], Chiara Mazzi[a,b,*], Elisabetta Colombari[a,b], Antonio M. Chiarelli[c], Brian A. Metzger[d], Carlo A. Marzi[a], Silvia Savazzi[a,b]

[a] Department of Neuroscience, Biomedicine and Movement Sciences, University of Verona, Strada le Grazie 8, Verona, Italy
[b] Perception and Awareness (PandA) Laboratory, Department of Neuroscience, Biomedicine and Movement Sciences, University of Verona, Strada le Grazie 8, Verona, Italy
[c] Department of Neurosciences, Imaging and Clinical Sciences, University G. D'Annunzio of Chieti Pescara, Via dei Vestini 31, Chieti, Italy
[d] Department of Neurosurgery, Baylor College of Medicine, 1 Baylor Plaza, Houston, TX, USA

ARTICLE INFO

Keywords:
Visuospatial attention
Orienting
Reorienting
Optical imaging
EROS
Granger causality

ABSTRACT

The mechanisms of visuospatial attention are mediated by two distinct fronto-parietal networks: a bilateral dorsal network (DAN), involved in the voluntary orientation of visuospatial attention, and a ventral network (VAN), lateralized to the right hemisphere, involved in the reorienting of attention to unexpected, but relevant, stimuli. The present study consisted of two aims: 1) to characterize the spatio-temporal dynamics of attention and 2) to examine the predictive interactions between and within the two attention systems along with visual areas, by using fast optical imaging combined with Granger causality. Data were collected from young healthy participants performing a discrimination task in a Posner-like paradigm. Functional analyses revealed bilateral dorsal parietal (i.e. dorsal regions included in the DAN) and visual recruitment during orienting, highlighting a recursive predictive interplay between specific dorsal parietal regions and visual cortex. Moreover, we found that both attention networks are active during reorienting, together with visual cortex, highlighting a mutual interaction among dorsal and visual areas, which, in turn, predicts subsequent ventral activity. For attentional reorienting our findings indicate that dorsal and visual areas encode disengagement of attention from the attended location and trigger reorientation to the unexpected location. Ventral network activity could instead reflect post-perceptual maintenance of the internal model to generate and keep updated task-related expectations.

1. Introduction

Visual attention consists of those psychological and neural processes which mediate the processing of behaviorally relevant sensory information (Capotosto et al., 2012). Sensory information can be selected either through voluntary deployment of attentional control (goal-directed attention) or can be oriented or reoriented in response to novel or unexpected, but important, stimuli (stimulus-driven attention). An important point is that attention can be allocated in space not only overtly but also covertly, i.e. in absence of head or eyes movements. Also, covert attention can be directed towards either behaviorally significant locations or regions of space including unexpected but salient stimuli. In the case of visuospatial attention, goal-directed and stimulus-driven attention provide a typical system of selection of relevant information: sensory input at attended locations is directly enhanced, whereas at unattended positions a reorienting process is triggered to likely important stimuli (Natale et al., 2009).

Psychophysical assessment of covert orienting and reorienting is achievable by means of spatial cueing paradigms (Posner, 1980) in which a central symbolic cue (e.g. an arrow) provides relevant information about the location of an upcoming peripheral target. In the majority of trials (75–80% probability), this information is correct, i.e. the upcoming target is presented at the cued location (valid trials), whereas, in the minority of trials (25–20% of cases), the cue gives a wrong indication (invalid trials) as the target is presented at the uncued location (Capotosto et al., 2012; Doricchi et al., 2010; Natale et al., 2009; Vossel et al., 2006). Reaction time (RT) is typically faster in valid than invalid trials and the difference ("validity effect") represents an index of the time needed to disengage and shift attention from an attended to an unexpected, behaviorally relevant location (Posner, 1980).

From a neuroanatomical point of view, visuospatial attention mechanisms have been linked to parietal and frontal cortices (Corbetta et al., 2008; Corbetta and Shulman, 2002; Shomstein, 2012; Vossel et al., 2006). Specifically, it has been proposed that attentional orienting and

* Corresponding author at: Department of Neuroscience, Biomedicine and Movement Sciences, University of Verona, Strada le Grazie 8, I-37134 Verona, Italy.
E-mail address: chiara.mazzi@univr.it (C. Mazzi).

https://doi.org/10.1016/j.neuroimage.2020.117244
Received 3 April 2020; Received in revised form 5 June 2020; Accepted 3 August 2020
Available online 14 August 2020
1053-8119/© 2020 The Author(s). Published by Elsevier Inc. This is an open access article under the CC BY-NC-ND license.
(http://creativecommons.org/licenses/by-nc-nd/4.0/)

reorienting are regulated by two anatomically different, though functionally interconnected, cortical networks: a bilateral dorsal fronto-parietal (DAN) and a ventral fronto-parietal network (VAN). DAN, which becomes activated as top-down cues orient attention to specific locations (Corbetta et al., 2000, 2008), includes the intraparietal sulcus (IPS), the superior parietal lobule (SPL) and the frontal eye fields (FEF). In contrast, reorienting attention to unattended locations engages VAN. This network is lateralized to the right hemisphere and includes the temporo-parietal junction (TPJ) and the ventral frontal cortex (VFC) which mainly includes portions of the middle frontal gyrus (MFG) and the inferior frontal gyrus (IFG) (Corbetta et al., 2008).

It is generally accepted that DAN and VAN are characterized by anatomical segregation and functional specialization so that each of them subserves specific processes of allocation of attention (Vossel et al., 2014).

There is strong evidence about the exclusive role of DAN (especially IPS and SPL) in top-down attention orienting, and that parietal regions exert top-down attention-related modulation on striate and extrastriate visual areas (Bressler et al., 2008; Doesburg et al., 2016; Vossel et al., 2012). Conversely, the relationship between DAN and VAN and their respective contributions in the reorienting process are still not completely clear. More precisely, voluntary attentional orienting is thought to engage the dorsal network only while attentional reorienting would require an interaction between the two attention networks, however, the exact nature of this interaction is still debated (Corbetta et al., 2008; Vossel et al., 2014).

In fact, previous imaging studies looking at visuospatial attentional reorienting in response to invalid spatial cues have revealed activity in ventral regions and bilateral IPS (Vossel et al., 2006, 2012), and right SPL as well (Vossel et al., 2009). In agreement with these results, transcranial magnetic stimulation (TMS) studies (Capotosto et al., 2012; Chica et al., 2011) have shown the critical role of right IPS when attention is spatially reoriented to unattended but relevant stimuli. Although these findings strongly support the existence of an interplay between the DAN and VAN during spatial reorienting, little is known about the timing of this interaction. So far, the exact role of dorsal and ventral regions in attentional processes remains uncertain, as well as the predictive connections between them, especially in the different phases of attentional reorienting (disengaging, shifting and engaging attention; Posner, 1980).

Previous imaging studies have not provided enough information about the time-course of attentional processing, along with accurate localization of specifically activated cortical areas. To address this issue, techniques with both good temporal and spatial resolutions are needed. To date, the most widely employed techniques can achieve high resolution in just one dimension (i.e. space or time) and the only option has been to combine different methodologies (Gratton, 2010). Unfortunately, because of theoretic and technical mismatches between distinct techniques (Luck, 1999), this option cannot fulfill the goal of providing both spatial and temporal information on the cognitive process under study. To overcome this problem, optical imaging methods have begun to be employed. In particular, a relatively novel approach, named Event-Related Optical Signal (EROS) or Fast Optical Signal (FOS) (Chiarelli et al., 2013, 2014; Gratton et al., 1995; Gratton and Fabiani, 2001) represents an appropriate tool to address this question. Its main advantage is the ability to detect variations (i.e. fast optical signals) in optical scattering typical of the neural tissue when it is active, as opposed to when it is not (Gratton, 2010). EROS, availing of near-infrared light (NIR), detects reduction in the light-scattering which is associated with change in membrane potentials and with an increment of brain activities (Gratton et al., 1995). Thus, it provides a measure of neuronal activity with a high temporal localization power of less than 50 ms (Baniqued et al., 2013), which is close to what can be obtained with electroencephalography (EEG) and magnetoencephalography (MEG). Moreover, thanks to the geometry of the optical probes, the diffusion of detected NIR light that passed across the brain is restricted enough to obtain a sufficiently localized signal (on the order of cm), obtaining a spatial localization power superior to EEG and MEG and which reveals activity from extensive areas of the cortical surface (Gratton, 2010). This relatively new technique has been validated by many studies (Baniqued et al., 2013; Huang et al., 2013; Sable et al., 2007; Toscano et al., 2018) supporting its feasibility and reliability in investigating the dynamics of brain activations of specific cortical regions during the performance of cognitive operations (Gratton et al., 1997, 2000; Rykhlevskaia et al., 2006; Tse et al., 2013). In addition, the advantages of this technique can be maximized by combining EROS analyses with Granger causality. This association allows us to explore, not only the timing of activations of distinct brain areas but also to determine whether activity in one seed area is predictive of successive activity in other regions. Importantly, Granger causality calculates whether data from a defined area of interest in a specified temporal window can predict the values of another region activated in a subsequent timeframe (Roebroeck et al., 2005), thus revealing the direction of influences between selected regions of interest (ROIs). Granger's suitability for investigating directional relationships between brain regions in human cognition has already been assessed in previous fMRI, EEG and MEG studies (Bressler et al., 2008; Doesburg et al., 2016; Proulx et al., 2018). Considering that it is a statistical measure of directional influences between ROIs based solely on their temporal precedence (Roebroeck et al., 2005), its application to EROS, that has high temporal and spatial localization power, is ideal to improve our understanding about how information is shared between brain regions engaged in specific cognitive tasks.

In the present study, an endogenous spatial cueing paradigm was administered to healthy participants. In this kind of task, processing of valid and invalid trials starts with the interpretation of the symbolic cue, followed by a voluntary allocation of attention and a cue-related orienting-response. This implies different operations: disengaging from a fixation point, shifting and engaging attention to the signaled location. In the case of invalid trials, the mismatch between attended and actual location of the target requires further attentional mechanisms, namely, disengaging, shifting and re-engaging attention to the correct location (Natale et al., 2009).

By coupling this behavioral approach with EROS and Granger causality, capable of identifying the timing of activation in definite brain regions and to unveil the predictive relationship among them, the present study aims at characterizing the neural spatio-temporal dynamics of attentional processes. In particular, exclusively focusing on parietal and temporal cortices, we sought to trace the time-course of brain activations in posterior nodes of the DAN and VAN to clarify the different roles of dorsal and ventral regions in attentional orienting and reorienting.

2. Material and methods

2.1. Participants

A total of twenty-nine right-handed (as assessed by the Edinburgh Handedness Inventory, Oldfield, 1971) adults, were recruited for the study and received compensation for their participation. All reported normal or corrected-to-normal visual acuity and no history of neurological or psychiatric disorders. All but two (authors G.P. and E.C.) were naïve to the goals of the study.

All participants gave their written informed consent before participating in the study, which was conducted in accordance with the 2013 declaration of Helsinki and approved by the Ethics Committee of the European Research Council and of the Verona Azienda Ospedaliera Universitaria Integrata (AOUI). Data from 8 participants were excluded from the analysis because of technical difficulties during imaging data acquisition, such as digitization issues (2 participants), low scattering parameters due to dark skin and hair (2 participants) or an insufficient number of good channels caused by detector overvoltage (4 participants). The rate of participants' exclusion, due to imaging acquisition issues, appears to be higher than that typically found in EROS studies. In this

case, EROS setup and optical data recording have required a little refinement during the first period of data collection, thus engendering a higher rate of data exclusion than usual.

Moreover, data from other 3 participants were discarded as behavioral task outliers. The final sample was thus composed of eighteen participants (3 males, mean age ± standard deviation: 24 ± 3.7).

2.2. Experimental procedure

The whole experiment included two sessions performed over two separate days. These sessions were identical in setting and behavioral conditions (type of task, number of blocks and trials), except for EROS montages (see below). The experiment was divided into two sessions in order to obtain an adequate number of trials while avoiding fatigue for participants.

In total, each session lasted about three and a half hours, which included EROS setup, optical data recording during the behavioral task, and co-registration procedures consisting of the digitization of optode scalp locations.

2.3. Behavioral task

Participants were tested in a dark testing room. During the experimental sessions, they sat in front of a 17 in. LCD monitor (resolution 1920 × 1080, refresh rate of 144 Hz) placed at a viewing distance of 57 cm, with head laying on an adaptable chin rest so that eyes could be aligned with the center of the screen.

A modified version of an endogenous spatial attention cueing paradigm (Posner, 1980), was employed (see Fig. 1A).

Each trial began with the presentation of a central black fixation cross, followed 500 ms later by a central predictive cue presented for 200 ms above the fixation point. After a variable randomized interval, lasting between 300 and 600 ms, the cue disappeared and was immediately followed by target onset (a vertical or horizontal, black-and-white, 2° square grating) presented at an eccentricity of 2° from the fixation cross to the inner edge, along the horizontal meridian. Participants were instructed to deploy their attention to the side indicated by the cue while maintaining their gaze on the central fixation cross throughout the block. Targets were presented for 150 ms after which, they were to discriminate as fast and as accurately as possible the orientation of the target by pressing one of two buttons of a response box with the index for horizontal targets or with the middle finger for vertical targets.

In each block, horizontal and vertical gratings randomly occurred with the same probability. Moreover, trials could be valid (75%), that is when the target was presented to the cued visual hemifield, or invalid (25%), when the target was presented to the uncued visual hemifield.

Each experimental session was composed of 24 blocks (for a total of 48 blocks per participant). The cue direction was consistent throughout a block: in half of the blocks (n = 12) it pointed to the right, while, in the other half, to the left visual hemifield. The order of blocks was alternated in each experimental session.

Each block consisted of 64 trials for a total of 3072 trials (2304 valid, 768 invalid) per participant. Participants could rest during inter-block intervals and could initiate the next block by pressing a key.

2.4. Optical recording

EROS data were recorded for the entire behavioral experiment, using two synchronized Imagent frequency domain systems (ISS, Inc., Champaign, IL). Thirty-two laser diodes emitted near-infrared light (830 nm) in a time-multiplexed scheme. The diodes were modulated at 110 MHz and the light was delivered into the brain through 400 μm silica optic fibers. The diffused light which exited from the head was detected by eight 3-mm fiber-optic bundles, connected to photomultiplier tubes (PMTs). Source and detector fibers were secured on the participant's head through a custom-built helmet, available in two different sizes. The PMT inputs were modulated at a slightly different frequency compared to laser diodes delivering a 3125 Hz cross-correlation frequency. Fast Fourier transform was applied to the PMTs output current in order to compute the DC intensity, AC amplitude and relative phase delay (source to detector) of the signal. In this study, only changes in phase delay data (converted into picoseconds delay) were analyzed.

For each helmet size, two different montages (see Fig. 1C) were used for the two sessions and combined during analyses providing dense coverage of the occipital and posterior temporo-parietal cortices, but not the frontal cortex (due to a limited number of available optodes). Each montage was to permit each detector to detect light from up to 16 time-multiplexed sources. In each montage sources and detectors were located in such a way as that a subset of sources could emit light simultaneously without causing cross-talk (light from multiple sources simultaneously recorded at a detector), resulting in 128 potential channels per session (with a minimum and maximum source-detector distance respectively of 17.5 and 50 mm; Gratton et al., 2000).

The cycle through each of the 16 multiplexed sets of sources lasted 25.6 ms (each source was switched on for 1.6 ms and off for 24 ms, in a fixed sequence) achieving a sampling rate of 39.0625 Hz.

Structural MRI scans were obtained for each participant. Scanning took place in a 1.5 Tesla Philips scanner at the Borgo Roma Hospital in Verona, using a standard 15-channel head coil. A whole brain high-resolution 3D T1-weighted image with magnetization-prepared rapid acquisition gradient echo (MPRAGE) was acquired with the following parameters: phase encoding direction= anterior to posterior, voxel size= 0.5 × 0.5 × 1 mm, Repetition Time= 7.7 ms, Echo Time= 3.5 ms, field of view= 250 × 250 mm, flip angle= 8°

Following each EROS session every source and detector holder location on the helmet, as well as fiducial points (nasion and pre-auricular points), were digitized using a neuronavigation software (SofTaxic, E.M.S., Bologna, Italy) combined with a 3D optical digitizer (Polaris Vicra, NDI, Waterloo, Canada).

The digitized scalp optical locations were co-registered with the structural MR images using a method implemented in an OCP software package (Optimized Co-registration Package, MATLAB code) developed by Chiarelli and colleagues (Chiarelli et al., 2015), and mainly based on scalp forcing and fiducial alignment procedures (Whalen et al., 2008). Finally, co-registered data were transformed to MNI space for the following analyses.

Continuous fast optical data were collected using the ISS Corporation "Boxy" program and preprocessed by means of P-POD (Pre-Processing of Optical Data, MATLAB code) an in-house software. The mean phase delay was adjusted to zero for each block. Data were then corrected for phase wrapping and de-trended to remove low-frequency drifts and baseline corrected. Before arterial pulse artifact was removed (45–200 heartbeat range) by using a regression algorithm (Gratton and Corballis, 1995), the phase of the modulated light was converted into time delay of the detected photons, expressed in picoseconds. A band-pass filter was then applied to remove frequencies below 0.5 Hz or above 15 Hz. Finally, the resultant data were segmented into epochs time-locked to the target onset and averaged separately for each participant, condition, and channel. The length of the epochs was different for the three EROS contrasts (see below *Section EROS analysis*): 1484 ms (486 ms before target onset and 998 ms after) for valid vs. baseline and invalid vs. baseline and 1535 ms (1280 ms before target onset and 255 ms after) for all vs. baseline.

Opt-3d custom software package (Gratton, 2000) was employed to compute statistics on functional data. Optical signals from source-detector channels whose diffusion path intersected a given voxel were averaged (Wolf et al., 2014). Phase delay data were baseline corrected using either a 200 ms pre-target interval or a 200 ms pre-cue interval (depending on the considered analysis, see Data analysis section) and spatially filtered with an 8-mm Gaussian kernel. Group-level t-statistics were computed across participants and then converted to z-scores for each voxel at each of the time points. Z-score maps, calculated from the

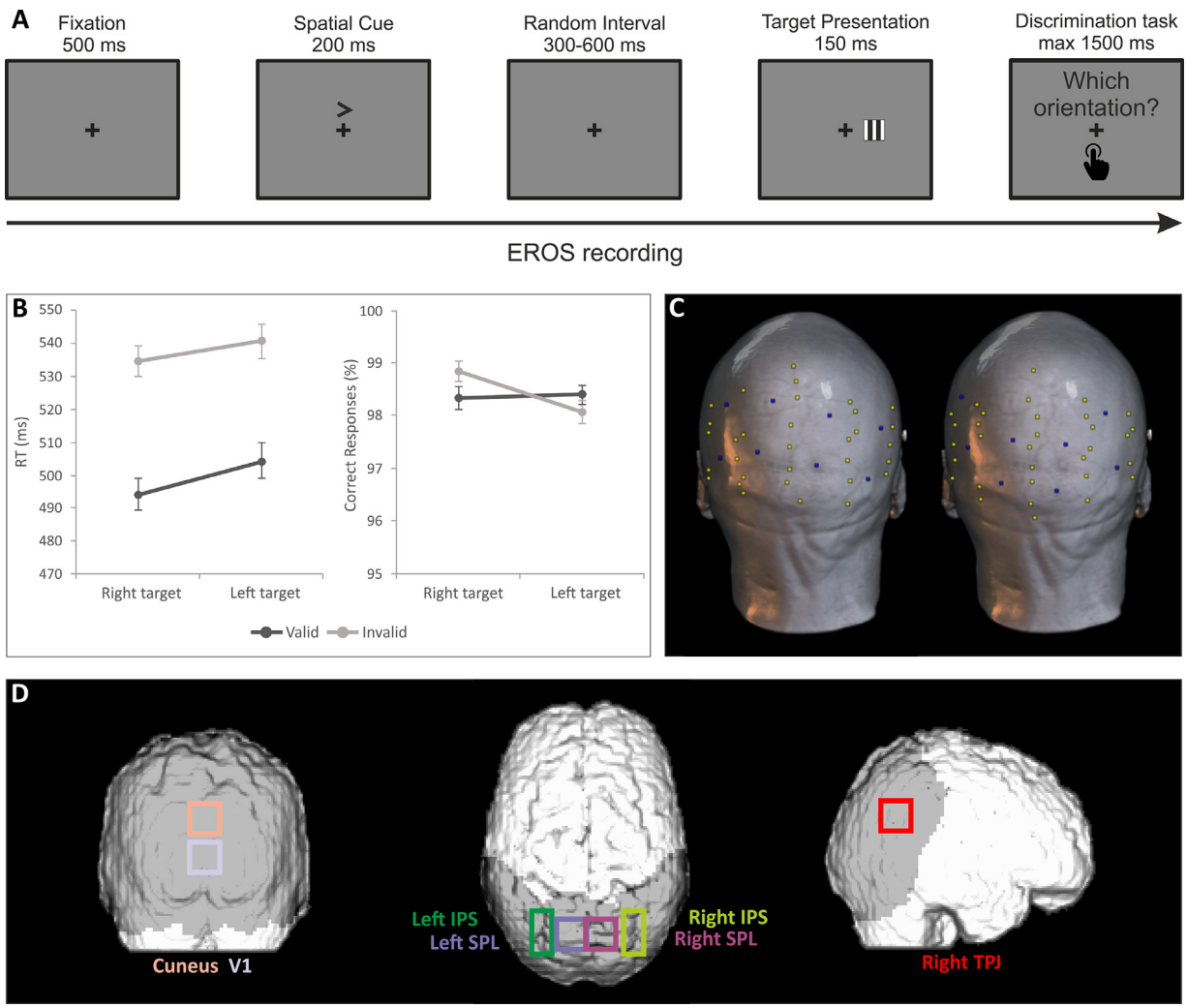

Fig. 1. Method and behavioral results.
(A) Experimental paradigm. A fixation cross was presented for 500 ms followed by a central informative cue lasting 200 ms. Participants were instructed to covertly direct attention to the side of space depicted by the cue. The target stimulus appeared after a random interval ranging from 300 to 600 ms and presented for 150 ms. Participants were then given 1500 ms to discriminate the target orientation (i.e. vertically or horizontally oriented gratings). In this example, a valid trial is shown (i.e. the cue points to the same visual hemifield in which the target subsequently occurs). (B) Behavioral results. Mean response times (left) and percentage of correct responses (right) are plotted as a function of whether the target appeared in the right or left hemifield (x-axis) and as a function of whether the attention cue was valid or invalid (separate lines). Error bars represent standard errors. (C) Optical montages. Two recording montages were used for each helmet size. Infrared optical sources (yellow dots) and detectors (blue dots) were placed to maximize recording coverage over parietal and occipital cortex. Here we show source and detector locations plotted onto the anatomical scan of a representative participant. (D) Selected ROIs. Estimated boundaries of the selected ROIs used for EROS and Granger analyses. ROIs are displayed in coronal (visual regions), axial (dorsal regions) and sagittal (ventral region) views as considered for statistical analyses and their coordinates are reported in Table 1.

p-value for each *t*-test, were corrected for multiple comparisons based on random field theory (Kiebel et al., 1999; Worsley et al., 1995). Subsequently, *Z*-scores were weighted and orthogonally projected onto images of the coronal, sagittal or axial surface of a template MNI brain, according to the physical homogenous model (Arridge and Schweiger, 1995; Gratton, 2000). See Supplementary Material: Fig. 1 for a schematic representation of the different steps to collect and process the data.

ROIs for the statistical analysis were selected both by inspection of the functional data and, more importantly, by selecting those areas found selectively activated in the literature on attentional control, in accordance with areas encompassed by EROS coverage (Fig. 1D). ROIs were thus placed along the posterior portion of DAN, i.e. left and right SPL (l/rSPL) and left and right IPS (l/rIPS), along the temporo-parietal portion of VAN, i.e. left and right TPJ (l/rTPJ) and within the occipital lobe, i.e. V1 and the dorsal portion of the cuneus. ROIs were identified relying on anatomical coordinates of parietal, temporal and occipital areas used in literature (e.g. Baniqued et al., 2018) and the correspondent Brodmann areas in which these regions are known to be included (i.e. BA7 for SPL, the intersection of BA7 and BA39 for IPS, BA39 for TPJ, BA17 for V1, BA 18 and 19 for cuneus). Specifically, the Yale online search tool (http://sprout022.sprout.yale.edu/mni2tal/mni2tal.html) was used to define ROIs boundaries in order to prevent or reduce overlap of different ROIs, given that the considered areas are contiguous in the human brain (see Table 1). All the ROIs were defined by a 2-dimensional box-shaped structure (the third dimension is missing as the optical signal is projected on the brain surface). See Table 1 where only two dimensions are listed for ROIs that were analyzed using separately axial (x, y), sagittal (y, z) or coronal projections (x, z).

2.5. Data analysis

2.5.1. Behavioral data

Data were processed using MATLAB 2013b and analyzed with IBM SPSS Statistics for Windows, version 22.

Table 1
MNI coordinates of selected ROIs.

Region	*Projection*	*Coordinates*			*Involved BA*
Right SPL	Axial	*x* =	0	20	7
		y =	−84	−64	
Left SPL	Axial	*x* =	−20	0	7
		y =	−84	−64	
Right IPS	Axial	*x* =	26	40	7–39
		y =	−87	−59	
Left IPS	Axial	*x* =	−36	−22	7–39
		y =	−87	−59	
Right TPJ	Sagittal	*y* =	−69	−49	39
		z =	21	41	
V1	Coronal	*x* =	−10	10	17
		z =	−4	16	
Cuneus	Coronal	*x* =	−10	10	18–19
		z =	20	40	

For each participant, horizontal and vertical trials were systematically collapsed. Mean reaction times (RTs), accuracy rates and the corresponding standard deviations (SDs) were measured for each of the four behavioral conditions (right target valid – invalid, left target valid – invalid) across participants. Trials with RTs exceeding ±3SDs from the mean, in each condition, were considered as outliers and removed from the analyses.

Mean RTs and mean percentage of correct responses were then entered in two separate repeated-measures analyses of variance (ANOVA) with *cue side* (right/left) and *target side* (right/left) as within-subject factors.

2.5.2. Functional data

EROS analysis: the dependent variable for optical data analyses was change in phase delay from baseline, averaged for each participant and condition. One-tailed tests were carried out on the voxel with the maximum delay value in each ROI, at each latency. Significant activity was found if ROI peak Z scores reached statistical significance ($p < 0.05$), adjusted for multiple comparisons (Kiebel et al., 1999; Worsley et al., 1995).

Trials with horizontal and vertical gratings were collapsed and three main contrasts were chosen for statistical analyses: all (valid and invalid) versus baseline, valid versus baseline, and invalid versus baseline. In the first contrast (all versus baseline), in which latencies ranging between −332 ms and 0 ms were considered, all trials were collapsed together and contrasted against baseline (i.e. a 200 ms time window preceding cue onset: from −1024 to −819 ms). Generally, since attentional deployment processes begin at about 200 ms after cue presentation, and our cue-target interval was variably randomized among trials (from 300 to 600 ms), in our pre-target analysis we selected that specific time window in order to be sure it was enough homogenous to the orienting response. In the other two contrast (valid versus baseline and invalid versus baseline), in which functional activity was observed from 0 ms to 767 ms, valid trials and invalid trials were contrasted against baseline (the 200 ms preceding the target onset), independently from visual hemifield.

Granger causality: forward Granger causality analysis was computed in order to examine the predictive relationship among activations in different areas at different time-lags. This analysis relies on the extrapolation of a meaningful seed within an ROI consisting of a time window that will be compared to another window of the same duration. Specifically, this approach investigates whether the activity of the seed ROI predicts the activity in the other ROIs at a later time-lag, on the basis of the similarity in data shape. In other words, using two different linear regression models (the restricted and the unrestricted model), Granger causality calculates the improvement in the prediction of one brain region's signal results from another temporally earlier region's signal. Importantly, this is done at the individual level allowing for variability in timing between subjects and ensuring the identification of complex patterns which may not be evident in the across-participants conventional EROS analyses. The resulting statistical maps are thus based on the average of individual values calculated separately per ROI and contrast. Maps were derived from computation of *t statistics* and transformation into *z scores*, running this procedure for each lag. Then, a correction for multiple comparisons was applied within each ROI, by means of the same random field theory techniques (Worsley et al., 1995; Kiebel et al., 1999) used for EROS analysis. Predicted ROI activity was observed in 15 time-lags which correspond to the same time points used in EROS analyses. Starting from lag 0 (corresponding to 0 ms) all the other lags were divided by 25.6 ms, namely the sampling rate, until reaching the last lag which corresponds to 358 ms. If a significant predicted activation at a specific lag (i.e. z-score exceeded the criterion value $p < 0.05$) was found, on the basis of that lag and the selected seed, the predicted and subsequent time window containing the predicted ROI peak activation, was measured. For valid and invalid versus baseline contrasts, the considered critical time window started from target onset onwards, according to the selected seed. As to the all versus baseline contrast, the time points comprising the 400 ms before target onset were taken into account. Even though we firstly focalized on lags in line with our EROS results, we then carried out exploratory analyses to probe effects in each lag and ROI.

3. Results

3.1. Behavioral results

The repeated-measure ANOVA conducted on mean RTs showed a significant main effect of *target side* ($F(1,17) = 7.528$, $p < 0.05$, $\eta p^2 = 0.307$), with participants faster in discriminating the target on the right (514 ms) than on the left side of the screen (522 ms). No significant difference of *cue side* was found ($F(1,17) = 1.163$, $p = 0.296$, $\eta p2 = 0.064$). Importantly, the interaction between *cue side* and *target side* was significant ($F(1,17) = 101.486$, $p < 0.01$, $\eta p^2 = 0.857$). To further investigate this effect, a paired-samples (two-tailed) *t*-test was carried out by comparing mean RTs for valid (499 ms) and invalid trials (538 ms). This analysis reached statistical significance ($t(17) = -10.074$, $p < 0.01$) indicating that the valid condition was associated with faster RTs, thus showing an attentional orienting benefit in target discrimination (Fig. 1B).

The repeated-measure ANOVA on mean percentage of correct responses showed significant main effects of both *cue* ($F(1,17) = 9.435$, $p < 0.01$, $\eta p^2 = 0.357$) and *target* ($F(1,17) = 10.557$, $p < 0.01$, $\eta p^2 = 0.383$), indicating that participants were more accurate when the cue pointed to the left side of the screen (left 98.6%, right 98.2%) and the target was on the right (left 98.2%, right 98.6%,), in line with the results observed in the RTs analysis. However, the interaction between *cue* and *target* was not statistically significant ($F(1,17) = 1.077$, $p = 0.314$, $\eta p^2 = 0.060$).

3.2. Functional results

3.2.1. Orienting process

To investigate the spatiotemporal dynamics of attentional orienting, we conducted two EROS contrasts: all versus baseline (Fig. 2A) and valid versus baseline (Fig. 2B). In the former, we found a significantly larger activation within the selected ROIs from 300 ms prior to target onset. In the latter, we found greater activations yielded by valid trials compared to the baseline condition, in the time window ranging from target onset to 767 ms post target.

Prior to target onset: we first looked at the all versus baseline contrast. Relative to baseline, we found a significant increase of activation in V1 at 204 ms ($z = 2.88$; $z\ crit = 2.55$) before target onset (Fig. 2A). This was followed by significant activity in lSPL at about −180 ms ($z = 2.35$; $z\ crit = 2.29$), increased activity in rSPL ($z = 2.78$; $z\ crit = 2.76$), lSPL ($z = 2.5$; $z\ crit = 2.38$), and lIPS ($z = 2.53$; $z\ crit = 2.35$) 153 ms before target onset, and finally greater activity was observed in lSPL at −76

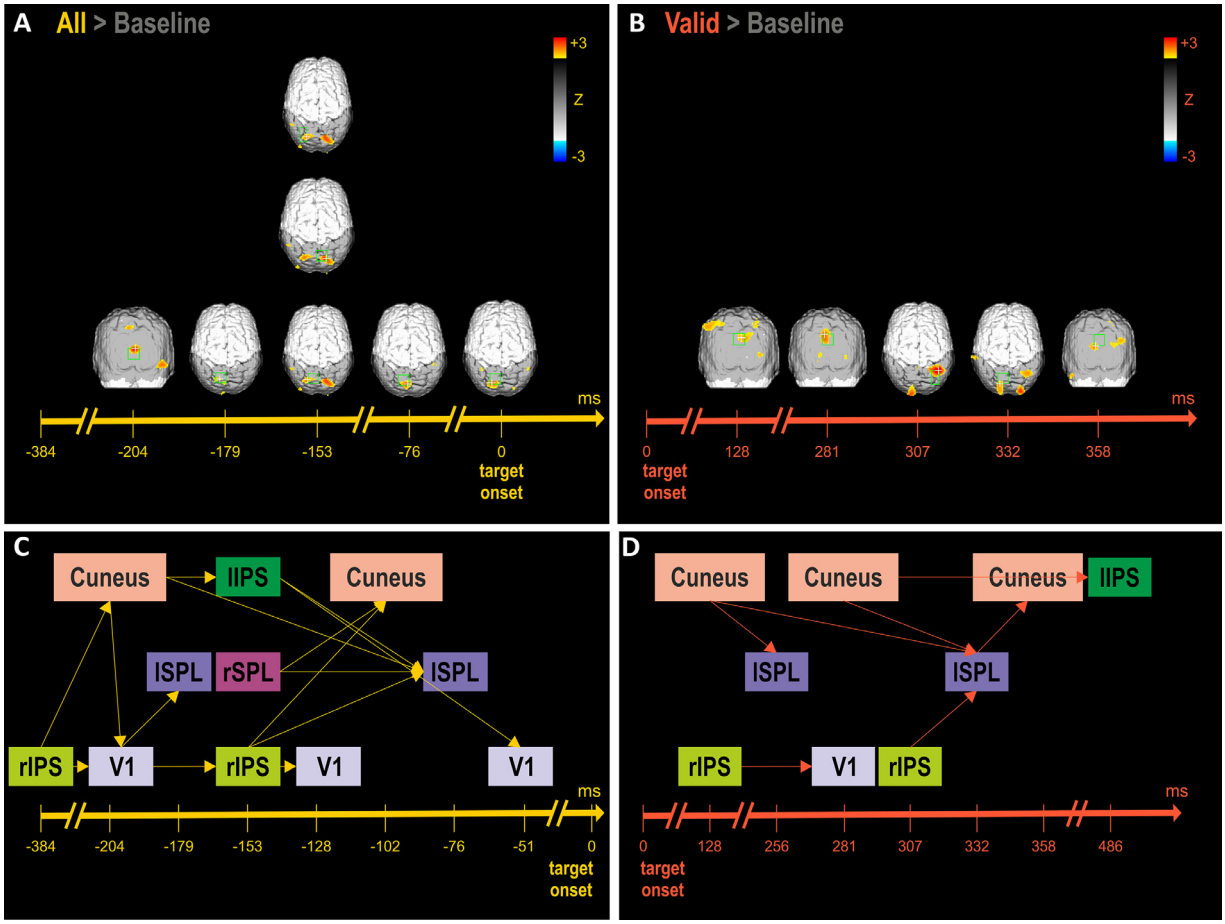

Fig. 2. EROS orienting effects and Granger results.
(A) EROS orienting effects before the target onset. Significant statistical parametric maps of the z-score difference between all trials and baseline (corresponding to the 200 ms time window preceding the cue onset) are depicted (activation threshold z-score = 2.0 uncorrected). Each map represents a 25.6 ms interval, within the 384 ms preceding target onset, in which significant effects occurred in selected ROIs (green boxes). The white cross within each ROI shows the peak voxel. (B) EROS orienting effects after target onset. Significant statistical parametric maps of the z-score difference between valid trials and baseline (corresponding to the 200 ms preceding the target onset) are depicted (activation threshold z-score = 2.0 uncorrected). Each map represents a 25.6 ms interval of the 767 ms after target onset, in which significant effects occurred in selected ROIs (green boxes). The white cross within each ROI shows the peak voxel. (C) Granger causality results on all versus baseline contrast, (D) Granger causality results on valid versus baseline contrast. For these analyses all dorsal and visual ROIs were chosen as seeds at different time lags. In these schemes, each colored box corresponds to a specific ROI. Each arrow indicates a significant predictive link between the starting box, representing the seed ROI at a precise time lag, and the matched box, representing the predicted ROI at a subsequent time lag (see Table 2). The values reported on the timeline refer to the peak activity within the considered time interval for each ROI.

(z = 2.67; z *crit* = 2.39) and 0 ms (z = 2.67; z *crit* = 2.42). See Supplementary Material: Fig. 2A for time traces of the mean activation of each ROI in all versus baseline contrast.

After target onset: when valid trials were contrasted versus baseline, there was an increase of activation in the dorsal portion of the cuneus at both 128 (z = 2.41; z *crit* = 2.36) and 281 ms (z = 2.66; z *crit* = 2.25) after target onset (Fig. 2B). Subsequently, rIPS revealed stronger activation at a latency of 307 ms (z = 3.27; z *crit* = 2.62), while at 332 ms (z = 2.46; z *crit* = 2.42) a significant increase of activation was elicited in lSPL. Finally, greater cuneus activity was observed at 358 ms (z = 2.5; z *crit* = 2.31). See Supplementary Material: Fig. 2B for time traces of the mean activation of each ROI in valid versus baseline contrast.

Overall, these results are in keeping with evidence that orienting of attention engages a bilateral dorsal system along with visual areas. In this contrast, visual areas reveal a more sustained activity pattern compared to the time interval preceding target onset, as it can be seen by greater activations in cuneus at several time lags, which, indeed, do not significantly emerge in the previous EROS contrast investigating activity prior to target onset.

Granger causality - prior to target onset: we performed Granger causality analyses to better understand the predictive interplay between areas. Since Granger causality enables us to detect also significant activity patterns not shown by typical EROS analysis, we integrated EROS data by using as seeds those ROIs which activity was found to be predicted by activity in other ROIs used as seeds in earlier time points. In this manner, we could highlight the cascade of predictive activity among neural areas by following the different timings of their engagement. With Granger causality on all versus baseline contrast, we assessed the predictive interactions over time in the cue-to-target interval. Results revealed a consistent continuous reciprocal pattern of prediction between dorsal and visual areas (Fig. 2C). Specifically, activity in rIPS (peak activation −384 ms) was predictive of activity in V1 and dorsal cuneus (peak activation −204 ms), which in turn was predictive of activity in dorsal parietal areas including lSPL (peak activation −179), lIPS, and rIPS (peak activation −153). This stream of predictive influences terminates in visual areas (such as V1 and cuneus) and in lSPL in which predicted orienting activity corresponds to a peak at −51, −102 and −76 ms respectively (see Table 2 for significant lags and the corresponding time windows).

Table 2
Granger analyses – orienting results.

Seed ROI	*Seed Interval (ms)*	*Peak Activity (ms)*	*Predicted ROI(s) (PR)*	*PR Interval (ms)*	*PR Peak Activity (ms)*	*Sig. Lag*	*Statistics*
Prior target onset							
rIPS	512 - 332	384	V1	307 - 128	204	179	z = 3.14 z *crit*= 2.68
			Cuneus	256 - 102	204	127	z = 2.49 z *crit*= 2.38
Cuneus	256 - 102	204	V1	307 - 128	204	25	z = 3.48 z *crit*= 2.65
			lIPS	204 - 76	153	25	z = 2.72 z *crit*= 2.57
			lSPL	153 - 25	76	25	z = 3.38 z *crit*= 2.56
V1	307 - 128	204	lSPL		179	25	z = 3.83 z *crit*= 2.55
			rIPS	230 - 102	153	25	z = 3.02 z *crit*= 2.74
lIPS	204 - 76	153	V1	179 - 76	128	25	z = 2.88 z *crit*= 2.65
			lSPL	153 - 25	76	25	z = 3.97 z *crit*= 2.69
rSPL	230 - 102	153	Cuneus	153 - 51	102	76	z = 2.90 z *crit*= 2.73
			lSPL	153 - 25	76	25	z = 2.90 z *crit*= 2.58
rIPS	230 - 102	153	Cuneus	153 - 51	102	76	z = 2.90 z *crit*= 2.73
			lSPL	153 - 25	76	25	z = 2.90 z *crit*= 2.58
			V1	179 - 76	51	25	z = 3.12 z *crit*= 2.68
After target onset							
rIPS	51 - 204	127	V1	230 - 358	281	76	z = 3.24 z *crit*= 3.11
Cuneus	25 - 179	127	lSPL	204 - 307	256	204	z = 3.24 z *crit*= 3.11
			lSPL	281 - 384	332	230	z = 3.31 z *crit*= 3.19
Cuneus	204 - 332	281	lSPL	281 - 384	332	76	z = 3.27 z *crit*= 3.12
			lIPS	409 - 537	486	230	z = 3.40 z *crit*= 3.01
rIPS	255 - 383	307	lSPL	281 - 384	332	25	z = 3.10 z *crit*= 3.02
lSPL	281 - 384	332	Cuneus	307 - 409	358	25	z = 4.22 z *crit*= 3.19

Granger causality - after target onset: Granger causality conducted on valid versus baseline contrast (analyzing the time window after target onset) revealed a similar recurrent activation pattern in which dorsal and visual areas mutually predict each other (Fig. 2D). In particular, earlier in time, activity in rIPS and cuneus (peak activation 127 ms) were predictive of activity in V1 and lSPL (peak activation 256 and 281 ms, respectively). Given peak activation of 281 in cuneus, this predicts peak activation firstly in lSPL (at 332 ms post-target onset), which, in turn, predicts peak activation in cuneus (at 358 ms post-target onset), and secondly, in lIPS at a later lag (at 486 ms post-target onset; see Table 2 for significant lags, the corresponding time windows, and statistics).

Overall, our findings suggest a clear involvement of a bilateral dorsal system along with visual areas in attentional orienting. Specifically, our data indicate a two-way predictive relationship among dorsal and visual areas activations, mainly involving a recursive predictive relationship between rIPS and V1 activations in both contrasts, and between cuneus and lSPL, especially in the valid versus baseline contrast.

3.2.2. Reorienting process

To investigate the spatio-temporal dynamics of attentional reorienting, we contrasted invalid trials versus baseline, in which the analysis time frame ranged from target onset (i.e. 0 ms) to 767 ms post-target.

We found greater activity in cuneus at 102 (z = 2.83; z *crit* = 2.37) and 128 ms (z = 2.78; z *crit* = 2.14), in bilateral IPS at 204 ms (lIPS: z = 2.7; z *crit* = 2.46; rIPS: z = 2.36; z *crit* = 2.13) and in V1 at 358 ms (z = 2.68; z *crit* = 2.65), after target onset (Fig. 3A). Moreover, rTPJ and the cuneus revealed greater activity at 409 (z = 2.81; z *crit* = 2.56) and 435 ms (z = 3.2; z *crit* = 2.58). We also observed greater activity in rIPS at 435 (z = 2.79; z *crit* = 2.73), 486 (z = 2.57; z *crit* = 2.38), 537 (z = 2.6; z *crit* = 2.5), and 563 ms (z = 2.9; z *crit* = 2.55). Finally, we found significant activity in rTPJ activation at 588 (z = 2.8; z *crit* = 2.52) and 767 ms (z = 2.64; z *crit* = 2.43) after target onset. See Supplementary Material: Fig. 2C for time traces of the mean activation of each ROI in invalid versus baseline contrast. These findings suggest bilateral recruitment of dorsal regions in attentional reorienting, together with an involvement of right ventral and visual areas. Given the well-known importance attributed to rTPJ in attentional reorienting, we carried out an additional analysis in which we directly contrasted invalid against valid trials, observing its functional activity in the same time window (0–767 ms post target). We found significant activation in rTPJ at 409 (z = 3.21; z *crit* = 2.47), 435 (z = 3.42; z *crit* = 2.58), 588 (z = 2.47; z *crit* = 2.4), 742 (z = 2.7; z *crit* = 2.66) and 767 ms (z = 2.59; z *crit* = 2.46), in line with the activations found in the invalid versus baseline contrast.

We used Granger Causality analysis to study the predictive connections among dorsal, ventral and visual areas. Following the same logic as that adopted for previous Granger causality analyses, we selected different relevant seeds, whether significantly activated in EROS analysis, or not. Data showed an analogous pattern of prediction to that shown in orienting Granger causality: visual areas predict activity in dorsal areas and vice-versa. Specifically, a seed identified in cuneus at a range between 51 and 179 ms (peak activation 102 ms), predicts activity in rSPL corresponding to a peak at 409 ms, while dorsal regions, such as lIPS, lSPL, and rIPS (peak activation 204 ms) predict reorienting process in cuneus at two later lags inferring peaks at 307 and 409 ms (Fig. 3B). The most important difference respect to the orienting contrasts is the coming into play of rTPJ, which is, instead, absent in orienting processing. Indeed, several seed areas (cuneus, lIPS, lSPL, rSPL, and V1) predict activity in rTPJ with a peak activation at 435 ms, which, in turn, predicts activity in V1 and lIPS, both at the same later lag (peak activation 486 ms; see Table 3 for significant lags, the corresponding time windows and statistics).

Taken together, these findings underline, for attentional reorienting, a mutually predictive relationship between dorsal and visual areas, which occurs earlier in our time window. This link between dorsal and visual areas is followed by an involvement of ventral areas, specifically rTPJ, predicted by both dorsal and visual regions.

4. Discussion

This study aimed at uncovering the spatio-temporal dynamics of visuospatial attentional orienting and reorienting by means of non-invasive optical imaging i.e. a technique that combines a good temporal and spatial localization ability, thus representing an ideal tool to gather information on the time-course of activations of localized cortical areas during specific cognitive tasks. Additionally, in order to assess the predictive relationships between active brain areas at distinct stages of attentional processing, we adopted a Granger causality approach that enabled us to explain the predictive interplay among different regions by statistically predicting directed attentional effects of one ROI to another, subsequent in time.

Orienting and reorienting of attention are thought to be subserved by distinct neural systems connected to sensory regions and mainly situated

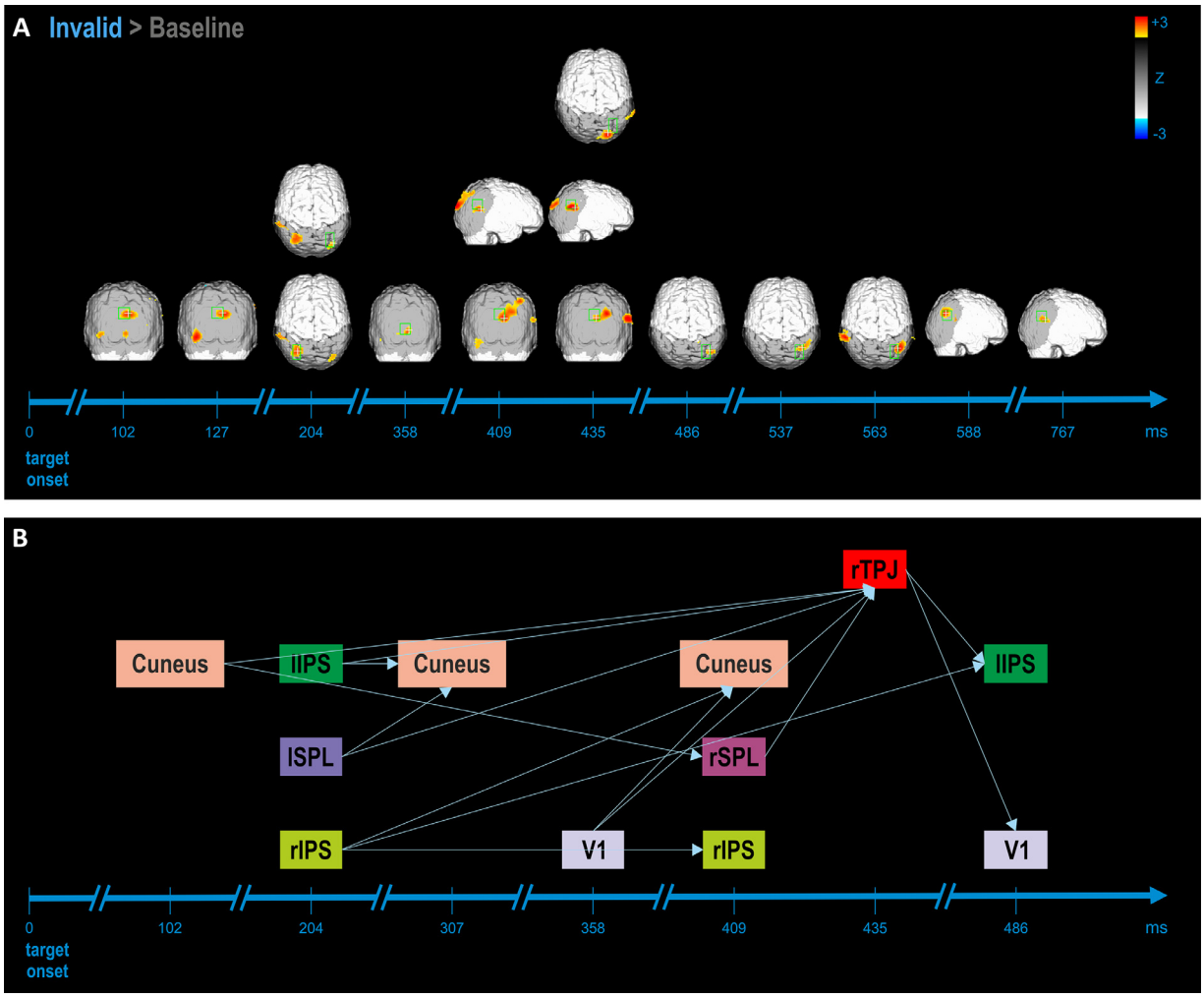

Fig. 3. Reorienting EROS effects and Granger results.
(A) EROS reorienting effect after the target onset. Significant statistical parametric maps of the z-score difference between invalid trials and baseline (corresponding to the 200 ms preceding the target onset) are depicted (activation threshold z-score = 2.0 uncorrected). Each map represents a 25.6 ms interval of the 767 ms after target onset, in which significant effects occurred in selected ROIs (green boxes). The white cross within each ROI shows the peak voxel. (B) Granger causality results on invalid versus baseline contrast. Predictive connections among dorsal, visual and ventral ROIs are illustrated. Again, each arrow indicates a significant predictive link between the starting box, representing the seed ROI at a precise time lag, and the matched box, representing the predicted ROI at a subsequent time lag (see Table 3). The values reported on the timeline refer to the peak activity within the considered time interval for each ROI.

Table 3
Granger analyses – reorienting results.

Seed ROI	*Seed Interval (ms)*	*Peak Activity (ms)*	*Predicted ROI(s) (PR)*	*PR Interval (ms)*	*PR Peak Activity(ms)*	*Sig. Lag*	*Statistics*
Cuneus	51 - 179	102	rSPL	332 - 486	409	255	$z = 3.31$ $z\ crit = 3.13$
			rTPJ	358 - 511	435	255	$z = 3.30$ $z\ crit = 3.25$
lIPS	153 - 281	204	Cuneus	204 - 383	307	25	$z = 3.19$ $z\ crit = 2.99$
			rTPJ	358 - 511	435	281	$z = 3.27$ $z\ crit = 3.12$
lSPL	153 - 281	204	Cuneus	204 - 383	307	25	$z = 3.19$ $z\ crit = 2.99$
			rTPJ	358 - 511	435	281	$z = 3.27$ $z\ crit = 3.12$
rIPS	127 - 255	204	Cuneus	332 - 511	409	204	$z = 3.74$ $z\ crit = 3.10$
			rIPS	307 - 486	409	255	$z = 3.68$ $z\ crit = 3.09$
			lIPS	409 - 537	486	358	$z = 3.33$ $z\ crit = 3.22$
V1	230 - 435	358	Cuneus	332 - 511	409	25	$z = 4.04$ $z\ crit = 2.95$
			rTPJ	358 - 511	435	25	$z = 4.08$ $z\ crit = 3.03$
rSPL	332 - 486	409	rTPJ	358 - 511	435	25	$z = 3.87$ $z\ crit = 3.08$
rTPJ	358 - 511	435	lIPS	409 - 537	486	51	$z = 3.16$ $z\ crit = 3.11$
			V1	435 - 563	486	76	$z = 3.22$ $z\ crit = 3.04$

in the parietal cortex: a bilateral dorsal and a right ventral network. Although there is strong evidence about the interaction between these systems during attentional tasks (Shomstein, 2012), a central but still unresolved question is to find out how this interaction occurs and how visual areas are involved.

4.1. Orienting

In the present work, attentional endogenous orienting (i.e. voluntary allocation of attention) was investigated by means of two EROS contrasts. The first, in which all trials (independently from validity condition) were compared with baseline, was intended to monitor the timing of activation of specific brain areas during deployment of attention between cue onset and target onset. The second, in which a comparison between valid trials and baseline was performed, was intended to study the spatio-temporal dynamics related to voluntary attentional orienting following target onset. Results from the two analyses were jointly taken into account to achieve a more exhaustive comprehension of the orienting and reorienting processes. Our findings are largely congruent with the literature (Chica et al., 2011; Corbetta et al., 2008; Kincade et al., 2005) by exhibiting an exclusive involvement of bilateral dorsal regions in endogenous orienting. The ventral network did not show any significant activation in this process while visual areas (BA 17, 18, 19) were actively involved, especially after target onset. With respect to the explored cue-target interval which provides insight into the attentional engagement to the cued spatial location, we found early activation of V1 followed by bilateral dorsal parietal activation. These findings suggest that the attentional engagement to the cued location is carried out by bilateral dorsal regions, which pre-activate V1 before the visual target appears. Neural activity is detected again in bilateral dorsal regions and in cuneus after target onset.

The contributions of dorsal parietal and visual areas during attentional orienting can be better explained by their predictive connections. Previous fMRI (Bressler et al., 2008; Lauritzen et al., 2009) and EROS experiments (Parks et al., 2015) have studied the connectivity between parietal and visual regions revealing a top-down influence from parietal (especially IPS) to early visual areas during sustained attention. Our Granger causality results are in accordance with these findings highlighting similar predictive patterns. Specifically, we found a recurrent tendency, for dorsal and visual areas to interact both in the cue-target and in the post-target period, in which, starting from rIPS, dorsal and visual regions mutually predict each other. Thus, the present evidence is in favor of the proposal of Vossel and colleagues (2012). By applying Dynamic Causal Modeling (DCM) to fMRI data the authors suggested a reciprocal causal influence from bilateral IPS to the corresponding bilateral visual areas. In line with this theoretical account derived from model testing, the continuous mutual prediction between rIPS and V1 is the more consistent trend emerging from our analyses. Interestingly, IPS has been shown (Jerde et al., 2012) to comprise prioritized maps of space which are organized in a retinal topographic manner, thus suggesting IPS as a reliable candidate in maintaining attention covertly. It is highly plausible that, thanks to this common retinotopic organization of IPS and V1, the predictive communication between these areas and the top-down influence exerted by IPS on V1 could be thought as the neural markers of sustained deployment of attention toward a previously cued location. Moreover, the other two areas, lSPL and cuneus, have been found to predict one another's activity at different time-lags after target onset. This is in line with previous evidence about the critical role of cuneus in visuospatial attention control (Doesburg et al., 2016), according to which the cuneus appears to be the target of a top-down attention information flow deriving from areas implicated in the orienting process (including dorsal areas).

Therefore, we suggest that two main flows of information are at work during the orienting process: one, subserving the interplay between IPS and V1 codes attentional orienting in a retinotopic manner and another, subserving the interplay between SPL and the dorsal portion of the cuneus (BA 18 and 19) codes orienting in a more spatiotopic manner, to provide information for the visuo-motor behavior elicited by the presentation of the target.

Taken together, our results suggest a predictive pattern between dorsal and visual regions that persists in both the analyzed functional contrasts, substantiating the existence of a dorsal and visual network involved in the supervision and elaboration of different processes of attentional orienting.

4.2. Reorienting

In the present experiment, we also investigated attentional endogenous reorienting, i.e. the cognitive process by which spatial attention is redirected to uncued location where behaviorally relevant events are presented. In order to analyze and separate the neural dynamics underlying attentional endogenous reorienting we implemented a functional contrast in which invalid trials were compared to the baseline in a post-target time window. Our results are in keeping with prior studies indicating a recruitment of both the dorsal and ventral attentional networks (Capotosto et al., 2012; Doricchi et al., 2010; Vossel et al., 2009) in conjunction with visual areas. However, while there is robust evidence for an interplay between the two attentional systems in the reorienting process (Vossel et al., 2014), it remains unclear how they interface with each other. In the current study, we endeavored to shed light on this issue by estimating the exact timing of activity in brain areas postulated to be critical in attentional reorienting. Moreover, we sought to understand the predictive roles of these areas depending on the different reorienting sub-processes. Dorsal and visual activation during attentional reorienting appears to follow a path along visual (BA 17, 18, 19) and dorsal regions (bilateral IPS) which show significant activations in alternating time intervals. Ventral activity during attentional reorienting showed greater activity in rTPJ occurring at several time-lags, quite later in time. These findings could be explained by referring to different functions in endogenous reorienting: dorsal and visual areas are engaged in earlier reorienting sub-processes (e.g. detecting a mismatch between cued and target location) while rTPJ is responsible for processes that occur later in time, thus not involved in triggering reorienting itself.

To extend upon the functional results, we applied Granger causality to our EROS reorienting analyses. At first glance, we noticed a similar activity pattern compared to that found with EROS: early in time, visual (BA 17, 18, 19) and dorsal regions (bilateral IPS and SPL) show significant activity alternating in subsequent time windows. In addition, the data suggest a functional link such that visual and dorsal regions influence each other in a post-target time window ranging between 100 and 400 ms. With respect to the predictive relationship with activity in rTPJ, almost all activated areas (with the exception of rIPS) exert predictive effects on rTPJ, which itself predicts activity in visual and dorsal regions. These data are partially in line with the previously cited fMRI study by Vossel and colleagues (2012). For attentional reorienting, these authors, by means of DCM, have reported significant connectivity from visual areas to rTPJ and from rTPJ to rIPS. On the one hand, we concur with Vossel et al's results about the disappearance of the recursive relationship between V1 and rIPS found to be fundamental in the orienting process and the general trend of connections. On the other, Vossel and colleagues (2012) have not highlighted an earlier functional link between visual and dorsal regions but have proposed an interpretation of the role of rTPJ namely, to inform the dorsal network of the violated top-down expectancy, which does not fit with our results. In the literature, there is a strong debate on the precise role played by rTPJ with regard to its interaction with the dorsal network in endogenous attentional reorienting. An early theory of how the two networks interact during attentional reorienting comes from Corbetta and Shulman (2002) and describes rTPJ as a circuit breaker, interrupting the ongoing selection in the dorsal network which, in turn, reorients attention to the unexpected, but relevant information. If that were the case, fast-latency signals from the ventral network should be sent to the DAN

to reorient attention. However, there is little evidence in the literature of fast-latency responses in the VAN preceding responses from the DAN (Corbetta et al., 2008). On the contrary, during attentional reorienting the signal from rTPJ tends to arise later in time compared to that of dorsal regions (Geng and Vossel, 2013). Importantly, rTPJ is mainly correlated with the P3b, a sub-component of the P300, which generally occurs in a late post-target time window (300–500 ms). Moreover, P3b is usually elicited by unexpected, but important, task-related events, corroborating the proposed link between P3b and rTPJ. By extension, another functional significance has been ascribed to P3b, namely that of "contextual updating" (Donchin and Coles, 1998; Polich, 2007). According to this theory, rTPJ should perform an updating of the internal model of the current environmental context as a function of incoming novel and unexpected information. This thesis fits with evidence about rTPJ activity in Posner attentional tasks in which invalid targets (strictly connected with rTPJ activation), being typically infrequent and unexpected, yield the updating of target-response pattern related to the likelihood of occurring of the subsequent targets (Geng and Vossel, 2013).

Our results are in favor of this post-perceptual interpretation of rTPJ, ruling out the idea of the ventral system as a "circuit-breaker" or a trigger of reorienting process. In fact, the first significant EROS activation of rTPJ during attentional reorienting was found later in time than visual and dorsal activations. Moreover, with Granger causality, we realized that all visual and dorsal regions predict rTPJ, likely coding the occurrence of something unexpected. From these data, it appears that the predictive and mutual interplay between visual and dorsal areas occurring earlier in time codes the mismatch between expectancy and reality and, at the same time, promotes the subsequent disengagement of attention from the cued location by triggering reorientation to the unexpected target location. rTPJ, predicted by visual and dorsal regions, does not take part in this reorienting process by emerging later in time. Rather, it initiates a post-perceptual evaluation of target information integrating novel information with the preexisting internal model. This interpretation of the role of the rTPJ is corroborated by evidence showing that it is repeatedly activated at later timeframes. Actually, the last significant rTPJ EROS activations occur about 600 ms after target onset, thus supporting the contextual updating theory, and suggesting that rTPJ terminates the updating process at those time-lags by modifying future task-related expectations.

5. Conclusions

The novelty of the present paper relies on the method used for investigating the dynamics underlying attentional processes. The combination of EROS and Granger causality allowed us to unravel functional relationships among specific brain areas, depending on their exact timing of activation in the processes of endogenous orienting and reorienting. With respect to attentional orienting, our results suggest a predictive pattern involving dorsal and visual regions both before and after target onset, suggesting the existence of a dorsal and visual network engaged in the supervision and manipulation of the various orienting sub-processes. As to reorienting, our results support a mutual interaction between visual and dorsal areas which, after encoding of the mismatch between expectation and reality, disengage attention from the cued location by triggering reorientation to the unexpected target. In contrast, the ventral network plays a post-perceptual role in updating the preexisting internal model as a function of novel incoming information on the unexpected target position, promoting adjustments about future task-related expectations. In conclusion, our findings refine and extend the existing knowledge of the neural bases of attentional processes.

The present study is limited by the extent of the investigated areas: our EROS montages, because of the number of sources and detectors at our disposal, were not sufficient to cover the frontal cortex not permitting to examine the activity of FEF and VFC, which are embedded in DAN and VAN, respectively. Evidence about their relevance in attentional processes and their connection to parietal regions, provides further details in the understanding of orienting and reorienting mechanisms. In particular, FEF is generally considered to cooperate with IPS in transmitting top-down modulation to the visual cortex during attentional orienting (Bressler et al., 2008; Vossel et al., 2012), although the effective direction of this cooperation remains unclear. As for the contribution of frontal regions to attentional reorienting, right MFG and right IFG emerge to be activated by invalid trials only (Vossel et al., 2006). Moreover, imaging evidence, revealed spontaneous activity in right MFG linked to both dorsal and ventral regions, showing the presence of neuronal populations related to both attentional networks (Fox et al., 2006) and providing further input to explain the functional interaction between systems underlying visuospatial attention.

Future studies should thus try to extend EROS montage to such frontal areas in order to investigate their role in both orienting and reorienting processes and to reveal their possible predictive role in triggering orienting responses towards other areas along the dorsal and ventral networks, also taking into account the possibility to combine EROS and Granger causality with other neuroimaging techniques (Tse et al., 2018; Xiao et al., 2020).

Declaration of Competing Interest

The authors declare that the research was conducted in the absence of any commercial or financial conflict of interest.

CRediT authorship contribution statement

Giorgia Parisi: Software, Formal analysis, Investigation, Writing - original draft. **Chiara Mazzi:** Conceptualization, Methodology, Software, Formal analysis, Writing - review & editing, Project administration. **Elisabetta Colombari:** Software, Formal analysis, Investigation, Writing - review & editing. **Antonio M. Chiarelli:** Software, Writing - review & editing. **Brian A. Metzger:** Conceptualization, Methodology, Software, Formal analysis, Writing - review & editing. **Carlo A. Marzi:** Conceptualization, Methodology, Writing - review & editing. **Silvia Savazzi:** Conceptualization, Methodology, Software, Formal analysis, Writing - review & editing, Supervision, Project administration.

Funding

This study was supported by European Research Council (ERC) [Grant number 339939 "Perceptual Awareness" P.I. CAM]. The funders had no role in the collection, analysis, and interpretation of data, in the writing of the report and in the decision to submit the article for publication.

Supplementary materials

Supplementary material associated with this article can be found, in the online version, at doi:10.1016/j.neuroimage.2020.117244.

References

Arridge, S.R., Schweiger, M., 1995. lt;title>Sensitivity to prior knowledge in optical tomographic reconstruction</title&gt. In: Chance, B., Alfano, R.R. (Eds.). In: Optical Tomography, Photon Migration, and Spectroscopy of Tissue and Model Media: Theory, Human Studies, and Instrumentation, 2389. SPIE, pp. 378–388. doi:10.1117/12.209988.

Baniqued, P.L., Low, K.A., Fabiani, M., Gratton, G., 2013. Frontoparietal traffic signals: a fast optical imaging study of preparatory dynamics in response mode switching. J. Cogn. Neurosci. 25 (6), 887–902. doi:10.1162/jocn_a_00341.

Baniqued, P.L., Low, K.A., Fletcher, M.A., Gratton, G., Fabiani, M., 2018. Shedding light on gray(ing) areas: connectivity and task switching dynamics in aging. Psychophysiology 55 (3), e12818. doi:10.1111/psyp.12818.

Bressler, S.L., Tang, W., Sylvester, C.M., Shulman, G.L., Corbetta, M., 2008. Top-down control of human visual cortex by frontal and parietal cortex in anticipatory visual spatial attention. J. Neurosci. 28 (40), 10056–10061. doi:10.1523/JNEUROSCI.1776-08.2008.

Capotosto, P., Babiloni, C., Romani, G.L., Corbetta, M., 2012. Differential contribution of right and left parietal cortex to the control of spatial attention: a simultaneous EEG-rTMS study. Cereb. Cortex 22 (2), 446–454. doi:10.1093/cercor/bhr127.

Chiarelli, A.M., Di Vacri, A., Romani, G.L., Merla, A., 2013. Fast optical signal in visual cortex: improving detection by general linear convolution model. Neuroimage 66, 194–202. doi:10.1016/j.neuroimage.2012.10.047.

Chiarelli, A.M., Maclin, E.L., Low, K.A., Fabiani, M., Gratton, G., 2015. Comparison of procedures for co-registering scalp-recording locations to anatomical magnetic resonance images. J. Biomed. Opt. 20 (1), 016009. doi:10.1117/1.jbo.20.1.016009.

Chiarelli, A.M., Romani, G.L., Merla, A., 2014. Fast optical signals in the sensorimotor cortex: general linear convolution model applied to multiple source-detector distance-based data. Neuroimage 85, 245–254. doi:10.1016/j.neuroimage.2013.07.021.

Chica, A.B., Bartolomeo, P., Valero-Cabré, A., 2011. Dorsal and ventral parietal contributions to spatial orienting in the human brain. J. Neurosci. 31 (22), 8143–8149. doi:10.1523/JNEUROSCI.5463-10.2010.

Corbetta, M., Kincade, J.M., Ollinger, J.M., McAvoy, M.P., Shulman, G.L., 2000. Voluntary orienting is dissociated from target detection in human posterior parietal cortex. Nat. Neurosci. 3 (3), 292–297. doi:10.1038/73009.

Corbetta, M., Patel, G., Shulman, G.L., 2008. The reorienting system of the human brain: from environment to theory of mind. Neuron 58 (Issue 3), 306–324. doi:10.1016/j.neuron.2008.04.017, Cell Press.

Corbetta, M., Shulman, G.L., 2002. Control of goal-directed and stimulus-driven attention in the brain. Nat. Rev. Neurosci. 3 (3), 201–215. doi:10.1038/nrn755.

Doesburg, S.M., Bedo, N., Ward, L.M., 2016. Top-down alpha oscillatory network interactions during visuospatial attention orienting. Neuroimage 132, 512–519. doi:10.1016/j.neuroimage.2016.02.076.

Donchin, E., Coles, M.G.H., 1998. Context updating and the P300. Behav. Brain Sci. 21 (1), 152–154. doi:10.1017/s0140525x98230950.

Doricchi, F., Macci, E., Silvetti, M., Macaluso, E., 2010. Neural correlates of the spatial and expectancy components of endogenous and stimulus-driven orienting of attention in the Posner task. Cereb. Cortex 20 (7), 1574–1585. doi:10.1093/cercor/bhp215.

Fox, M.D., Corbetta, M., Snyder, A.Z., Vincent, J.L., & Raichle, M.E. (2006). Spontaneous Neuronal Activity Distinguishes Human Dorsal and Ventral Attention Systems. www.pnas.orgcgidoi10.1073pnas.0604187103

Geng, J.J., Vossel, S., 2013. Re-evaluating the role of TPJ in attentional control: contextual updating? Neurosci. Biobehav. Rev. 37 (Issue 10), 2608–2620. doi:10.1016/j.neubiorev.2013.08.010, Pergamon.

Gratton, G., 2000. "Opt-cont" and "opt-3D": a software suite for the analysis and 3D reconstruction of the event-related optical signal (EROS). Psychophysiology 37.

Gratton, G., 2010. Fast optical imaging of human brain function. Front. Hum. Neurosci. 4, 52. doi:10.3389/fnhum.2010.00052.

Gratton, G., Corballis, P.M., 1995. Removing the heart from the brain: compensation for the pulse artifact in the photon migration signal. Psychophysiology 32 (3), 292–299. doi:10.1111/j.1469-8986.1995.tb02958.x.

Gratton, G., Corballis, P.M., Cho, E., Fabiani, M., Hood, D.C., 1995. Shades of gray matter: noninvasive optical images of human brain reponses during visual stimulation. Psychophysiology 32 (5), 505–509. doi:10.1111/j.1469-8986.1995.tb02102.x.

Gratton, G., Fabiani, M., 2001. The event-related optical signal: a new tool for studying brain function. Int. J. Psychophysiol. 42 (2), 109–121. doi:10.1016/S0167-8760(01)00161-1.

Gratton, G., Fabiani, M., Corballis, P.M., Hood, D.C., Goodman-Wood, M.R., Hirsch, J., Kim, K., Friedman, D., Gratton, E., 1997. Fast and localized event-related optical signals(EROS) in the human occipital cortex: comparisons with the visual evoked potential and fMRI. Neuroimage 6 (3), 168–180. doi:10.1006/nimg.1997.0298.

Gratton, G., Sarno, A., Maclin, E., Corballis, P.M., Fabiani, M., 2000. Toward noninvasive 3-D imaging of the time course of cortical activity: investigation of the depth of the event-related optical signal. Neuroimage 11 (5 I), 491–504. doi:10.1006/nimg.2000.0565.

Huang, J., Wang, S., Jia, S., Mo, D., Chen, H.C., 2013. Cortical dynamics of semantic processing during sentence comprehension: evidence from event-related optical signals. PLoS ONE 8 (8). doi:10.1371/journal.pone.0070671.

Jerde, T.A., Merriam, E.P., Riggall, A.C., Hedges, J.H., Curtis, C.E., 2012. Prioritized maps of space in human frontoparietal cortex. J. Neurosci. 32 (48), 17382–17390. doi:10.1523/JNEUROSCI.3810-12.2012.

Kiebel, S.J., Poline, J.B., Friston, K.J., Holmes, A.P., Worsley, K.J., 1999. Robust smoothness estimation in statistical parametric maps using standardized residuals from the general linear model. Neuroimage 10 (6), 756–766. doi:10.1006/nimg.1999.0508.

Kincade, J.M., Abrams, R.A., Astafiev, S.V., Shulman, G.L., Corbetta, M., 2005. An event-related functional magnetic resonance imaging study of voluntary and stimulus-driven orienting of attention. J. Neurosci. 25 (18), 4593–4604. doi:10.1523/JNEUROSCI.0236-05.2005.

Lauritzen, T.Z., D'Esposito, M., Heeger, D.J., Silver, M.A., 2009. Top-down flow of visual spatial attention signals from parietal to occipital cortex. J. Vis. 9 (13). doi:10.1167/9.13.18, 18–18.

Luck, S.J., 1999. Direct and indirect integration of event-related potentials, functional magnetic resonance images, and single-unit recordings. Hum. Brain Mapp. 8 (2–3), 115–120. doi:10.1002/(SICI)1097-0193(1999)8:2/3<115::AID-HBM8>3.0.CO;2-3.

Natale, E., Marzi, C.A., Macaluso, E., 2009. FMRI correlates of visuo-spatial reorienting investigated with an attention shifting double-cue paradigm. Hum. Brain Mapp. 30 (8), 2367–2381. doi:10.1002/hbm.20675.

Parks, N.A., Mazzi, C., Tapia, E., Savazzi, S., Fabiani, M., Gratton, G., Beck, D.M., 2015. The influence of posterior parietal cortex on extrastriate visual activity: a concurrent TMS and fast optical imaging study. Neuropsychologia 78, 153–158. doi:10.1016/j.neuropsychologia.2015.10.002.

Polich, J., 2007. Updating P300: an integrative theory of P3a and P3b. Clin. Neurophysiol. 118 (Issue 10), 2128–2148. doi:10.1016/j.clinph.2007.04.019, Elsevier.

Posner, M.I., 1980. Orienting of attention. Q. J. Exp. Psychol. 32 (1), 3–25. doi:10.1080/00335558008248231.

Proulx, N., Samadani, A.A., Chau, T., 2018. Quantifying fast optical signal and event-related potential relationships during a visual oddball task. Neuroimage 178, 119–128. doi:10.1016/j.neuroimage.2018.05.031.

Roebroeck, A., Formisano, E., Goebel, R., 2005. Mapping directed influence over the brain using Granger causality and fMRI. Neuroimage 25 (1), 230–242. doi:10.1016/j.neuroimage.2004.11.017.

Rykhlevskaia, E., Fabiani, M., Gratton, G., 2006. Lagged covariance structure models for studying functional connectivity in the brain. Neuroimage 30 (4), 1203–1218. doi:10.1016/j.neuroimage.2005.11.019.

Sable, J.J., Low, K.A., Whalen, C.J., Maclin, E.L., Fabiani, M., Gratton, G., 2007. Optical imaging of temporal integration in human auditory cortex. Eur. J. Neurosci. 25 (1), 298–306. doi:10.1111/j.1460-9568.2006.05255.x.

Shomstein, S., 2012. Cognitive functions of the posterior parietal cortex: top-down and bottom-up attentional control. Front. Integr. Neurosci. 6. doi:10.3389/fnint.2012.00038, (JULY 2012), 38.

Toscano, J.C., Anderson, N.D., Fabiani, M., Gratton, G., Garnsey, S.M., 2018. The time-course of cortical responses to speech revealed by fast optical imaging. Brain Lang. 184, 32–42. doi:10.1016/j.bandl.2018.06.006.

Tse, C.Y., Rinne, T., Ng, K.K., Penney, T.B., 2013. The functional role of the frontal cortex in pre-attentive auditory change detection. Neuroimage 83, 870–879. doi:10.1016/j.neuroimage.2013.07.037.

Tse, C.Y., Yip, L.Y., Lui, T.K.Y., Xiao, X.Z., Wang, Y., Chu, W.C.W., Parks, N.A., Chan, S.S.M., Neggers, S.F.W., 2018. Establishing the functional connectivity of the frontotemporal network in pre-attentive change detection with transcranial magnetic stimulation and event-related optical signal. Neuroimage 179, 403–413. doi:10.1016/j.neuroimage.2018.06.053.

Vossel, S., Geng, J.J., Fink, G.R., 2014. Dorsal and ventral attention systems: distinct neural circuits but collaborative roles. Neurosci. Rev. J. Bringing Neurobiol. Neurol. Psychiatry 20 (2), 150–159. doi:10.1177/1073858413494269.

Vossel, S., Thiel, C.M., Fink, G.R., 2006. Cue validity modulates the neural correlates of covert endogenous orienting of attention in parietal and frontal cortex. Neuroimage 32 (3), 1257–1264. doi:10.1016/j.neuroimage.2006.05.019.

Vossel, S., Weidner, R., Driver, J., Friston, K.J., Fink, G.R., 2012. Deconstructing the architecture of dorsal and ventral attention systems with dynamic causal modeling. J. Neurosci. 32 (31), 10637–10648. doi:10.1523/JNEUROSCI.0414-12.2012.

Vossel, S., Weidner, R., Thiel, C.M., Fink, G.R., 2009. What is "Odd" in Posner's location-cueing paradigm? Neural responses to unexpected location and feature changes compared. J. Cogn. Neurosci. 21 (1), 30–41. doi:10.1162/jocn.2009.21003.

Whalen, C., Maclin, E.L., Fabiani, M., Gratton, G., 2008. Validation of a method for coregistering scalp recording locations with 3D structural MR images. Hum. Brain Mapp. 29 (11), 1288–1301. doi:10.1002/hbm.20465.

Wolf, U., Wolf, M., Toronov, V., Michalos, A., Paunescu, L.A., Gratton, E., 2014. Detecting cerebral functional slow and fast signals by frequency-domain near-infrared spectroscopy using two different sensors. *Biomedical Optical Spectroscopy and Diagnostics* (2000). Paper TuF10 doi:10.1364/bosd.2000.tuf10.

Worsley, K.J., Poline, J.B., Vandal, A.C., Friston, K.J., 1995. Tests for distributed, nonfocal brain activations. Neuroimage 2 (3), 183–194. doi:10.1006/nimg.1995.1024.

Xiao, X., Shum, Y., Lui, T.K.-Y., Wang, Y., Cheung, A.T.-C., Chu, W.C.W., Neggers, S.F.W., Chan, S.S.-M., Tse, C., 2020. Functional connectivity of the frontotemporal network in preattentive detection of abstract changes: perturbs and observes with transcranial magnetic stimulation and event-related optical signal. Hum. Brain Mapp. doi:10.1002/hbm.24984, hbm.24984.